INCLUSIVE PUBLISHING
TRUSTED SCIENCE

PAPER • OPEN ACCESS

A long-chain based bromo and methyl substituted chalcone derivatives; experimental and theoretical approach on nonlinear optical single crystals

View the article online for updates and enhancements.
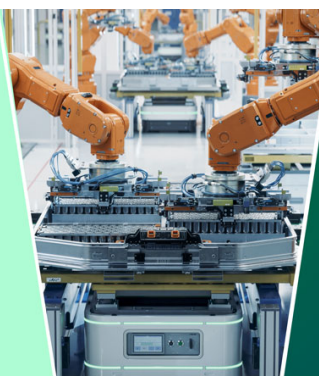
ECS
The **Electrochemical Society**
Advancing solid state & electrochemical science & technology

DISCOVER
how sustainability intersects with electrochemistry & solid state science research

Materials Research Express

A long-chain based bromo and methyl substituted chalcone derivatives; experimental and theoretical approach on nonlinear optical single crystals

Vinay Parol[1] , V Upadhyaya[2], A N Prabhu[1] , N K Lokanath[3] , Md Abu Taher[4] and Sri Ram G Naraharisetty[4]

1   Department of Physics, Manipal Institute of Technology, Manipal Academy of Higher Education, Manipal 576104, India
2   Manipal Centre for Natural Sciences, Manipal Academy of Higher Education, Manipal 576104, India
3   Department of Studies in Physics, Manasagangotri, University of Mysore, Mysuru 570006, India
4   School of Physics, University of Hyderabad, Hyderabad 500046, India

E-mail: ashwatha.prabhu@manipal.edu

Abstract

In the present work, growth of single crystals of chalcone derivatives {4-[(1E)-3-(4-methylphenyl)-3-oxoprop-1-en-1-yl]phenyl 4-methylbenzene-1-sulfonate} (**4M1PMS**) and {4-[(1E)-3-(4-bromophenyl)-3-oxoprop-1-en-1-yl]phenyl4-methylbenzene-1-sulfonate} (**4BPMS**), at room temperature is reported. The spectroscopic techniques are used to identify the presence of functional groups in the materials. The single-crystal XRD and powder XRD analysis reveals that 4M1PMS belongs to non-centrosymmetric ($P2_12_12_1$) and 4BPMS belongs to centrosymmetric ($P2_1/n$) crystalline system. The molecular structures exhibit C–H…O and $\pi...\pi$ intermolecular interactions. From UV/VIS/NIR spectroscopic studies, it is found that both samples have bathochromic shifts in linear absorbance (cut-off region) spectra. The broad emission region involved in several sharp emission peaks in blue region, exhibits a blue light emission property, as observed from photoluminescence study, in both the samples. The thermal stability of the materials were studied by TGA/DTA techniques and crystals were thermally stable until the melting point. In NLO study, 4M1PMS crystal has shown SHG efficiency 2.2 times that of KDP crystal. In addition, electronic contribution in hyperpolarizability (first order and second order) tensors of both the compounds were computed theoretically by M06-2X functional at DFT level. The open/closed aperture Z-scan technique were performed to evaluate third order nonlinear optical materials by measuring experimental parameters such as nonlinear absorption/refraction and calculate second-order hyperpolarizability with corresponding third-order nonlinear optical susceptibility ($\chi^{(3)}$) of 4M1PMS and 4BPMS. The surface damage threshold studies of 4M1PMS and 4BPMS were performed by Q-switched Nd:YAG laser at 532 nm.

1. Introduction

The field of Nonlinear Optics (NLO) emerged significantly after the invention of nonlinear optical material in 1970, and various optoelectronic materials prompted by many types of research for various technological applications [1–3]. The applications of organic materials have increased enormously over that of inorganic materials due to their distinct properties such as synthetic flexibility, high damage threshold value, low dielectric constant and ease of processability with an ultrafast response [4–6]. The low dielectric constant materials have reduced phase mismatch which is noteworthy for second harmonic generation (SHG). Therefore, these materials can have applications for frequency doubling, electro-optics modulation, optical parametric and terahertz wave generations [6–9]. Materials with third-order nonlinear optical response have better applicability feature in all-optical switching, power limiting and optical data storage applications [10–13]. The presence of

large NLO co-efficient in organic molecules is due to delocalization of π-electrons. Among organic materials, competent chalcone derivatives are the subclass of flavonoids, extensively studied for NLO application such as second harmonic and third harmonic generations. In addition, these materials are well established in biological activities such as anticancer [14], antifungal [15], antibacterial [16], and antimicrobial [17]. The chalcone derivatives consist of π- conjugation based molecular system with aromatic rings and equipped with donor/ acceptor electrons at the ends of the molecule. Aforementioned idea gives an increased attention to search new materials designed for various types of the molecular system such as D-π-D, D-π-A, A-π-A, D-π-A-π-D, A-π-D-π-A, and so on. These type of molecules have intermolecular charge transfer [18–20], which leads to high nonlinear optical hyperpolarizability. In the present investigation, synthesis of two chalcone derivatives, methyl-substituted (4M1PMS) and bromo substituted (4BPMS) materials is carried out. The selection of materials in the present study has the type D-π-A-π-D. Similar type of molecules (methoxy and chlorothiophene substituted chalcone derivatives) are reported by us [21, 22]. By changing/replacing the donor electron in the aromatic ring, 4M1PMS and 4BPMS have been synthesized successfully, crystallized by using solvent evaporation technique. As a part of extensive research on this class of compounds, a study of crystal growth and structure-related properties is also reported, apart from various characterization techniques (linear optical, thermal, and nonlinear optical properties). Furthermore, the computation framework is added to analyse dipole moment and polarizability parameters. In addition, electronic contribution of hyperpolarizability tensors (first order and second order) were calculated to show the eminence of the material for laser-assisted applications.

2. Experimental methods

2.1. Materials and their synthesis
The commercially available reagents and solvents are purchased from Sigma Aldrich and Molychem (with 96%–99% purity). The compounds were synthesized by Claisen Schmidt condensation reaction method. The synthesis of the materials (4M1PMS and 4BPMS) involves two steps: (1) synthesis of tosyloxy derivative (4-formylphenyl 4-methylbenzene-1-sulfonate) (2) synthesis of chalcone derivative materials (tosyloxy derivative to 4-methylacetophenone and tosyloxy derivative to 4-bromoacetophenone).

Step (1): Synthesis of tosyloxy derivative (aldehyde group): The initial compounds of 4 hydroxy benzaldehyde (1 mole) and 4-tolenesulphonyl chloride (1 mole) was dissolved in tetra hydro furan (THF) as a solvent. K_2CO_3 ($1/3^{rd}$ of 4-hydroxy aldehyde) was added gradually to the solution and reaction mixture was kept at 70 °C for 5 h. To avoid solvent evaporation, efficient cooling mechanism using glass condenser was adopted. After completion of the reaction, the final product was poured into ice-cold water and small quantity of 2 N HCl was added in order to maintain pH. All precipitations settled down at the bottom in 12 h. Tosyloxy derivative product was collected through filtration. The compound was dried at room temperature for 24 h. Further, thin layer chromatography (TLC) was performed to confirm the purity of the synthesized compound.
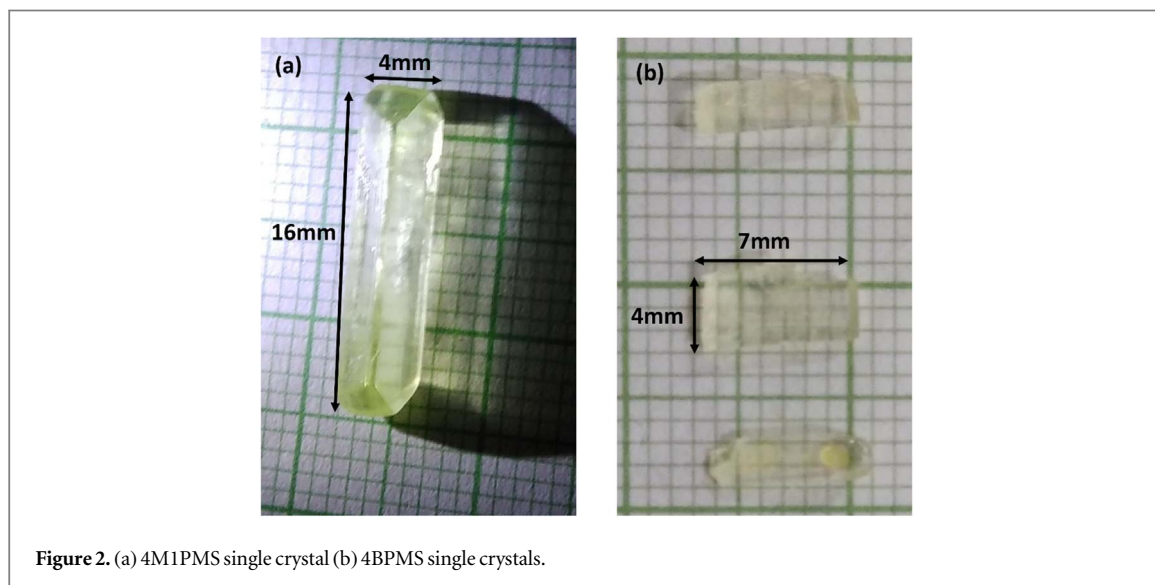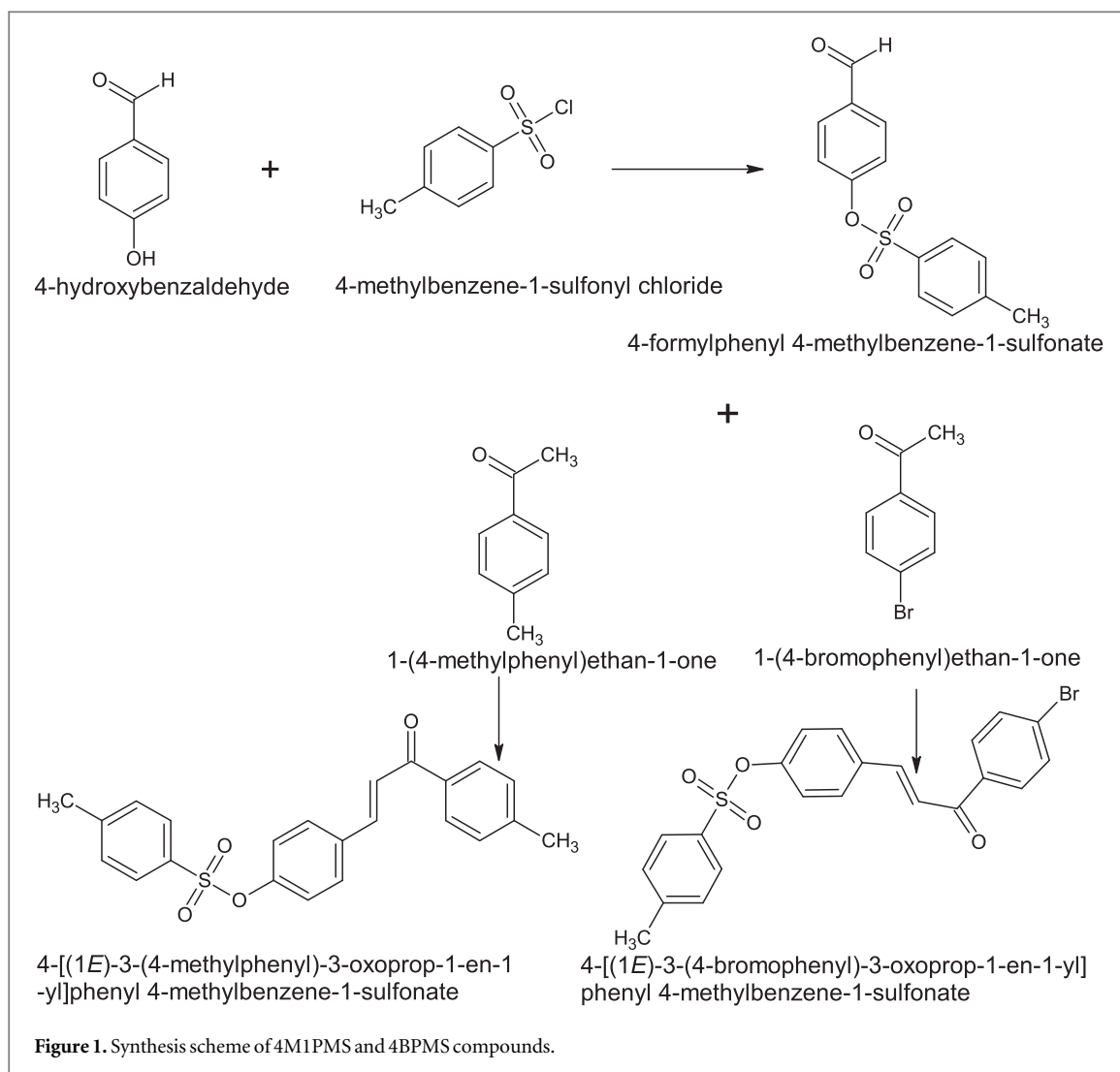
Step (2a): Synthesis of 4M1PMS: The tosyloxy aldehyde [4-formylphenyl 4-methylbenzene-1-sulfonate] (0.015 mole) and 4-methylacetophenone (0.015mole)] were dissolved in ethanol with gradual addition of NaOH (15%). **Step (2b): Synthesis of 4BPMS:** The mixture of 4-formylphenyl 4-methylbenzene-1-sulfonate (0.015 mole) and 4-bromoacetophenone (0.015mole) was dissolved in ethanol with a small addition of NaOH (10%). The solution mixtures of the two compounds were kept individually with a constant and continuous stirring for about 5 h and products were poured into ice-cold water. Further, resultant crude products were collected by vacuum filtrations, dried by suction and purified by recrystallizations in acetone. Scheme of synthesis for 4M1PMS and 4BPMS is shown in figure 1.

2.2. Growth of single crystals
Single crystals were grown by solvent evaporation technique. Advantages of this technique is simple and cost effective but selection of solvent plays a crucial role in solvent evaporation technique. Solvent is chosen based on the solubility of the material. The compounds are highly soluble in DMF (dimethylformamide) and chloroform but moderately soluble in acetone. Therefore, acetone is chosen as a prominent solvent for crystallizing 4M1PMS and 4BPMS. In order to grow single crystals, the saturated solution of 4M1PMS and 4BPMS were taken in a beaker covered with permeable sheet, kept under dust-free atmosphere. After 2–3 weeks, good quality of single crystals were obtained. The quality of the crystals were enhanced by repeated recrystallizations by using the same solvent (acetone). The grown single crystal are shown in figures 2(a) and (b).

2.3. Characterization techniques
The vibration frequencies corresponding to functional groups were identified using FT-IR and FT-Raman spectroscopic techniques. The mixtures of KBr (90%) and compounds (10%) were taken in pellet form for data collections. Vibrational modes corresponding to functional groups were obtained from Perkin-Elmer FT-IR

4-hydroxybenzaldehyde   4-methylbenzene-1-sulfonyl chloride

4-formylphenyl 4-methylbenzene-1-sulfonate

1-(4-methylphenyl)ethan-1-one   1-(4-bromophenyl)ethan-1-one

4-[(1*E*)-3-(4-methylphenyl)-3-oxoprop-1-en-1-yl]phenyl 4-methylbenzene-1-sulfonate

4-[(1*E*)-3-(4-bromophenyl)-3-oxoprop-1-en-1-yl]phenyl 4-methylbenzene-1-sulfonate

Figure 1. Synthesis scheme of 4M1PMS and 4BPMS compounds.

Figure 2. (a) 4M1PMS single crystal (b) 4BPMS single crystals.

and Bruker RFS 27 FT-Raman spectrometers between 4000 cm^{-1} to 400 cm^{-1}. Study of the hydrogen framework of the materials (4M1PMS and 4BPMS) were performed by dissolving the compounds individually in the DMSO (dimethyl sulfoxide) solvent, considering tetramethylsilane as an internal standard. The resultant spectrum and the corresponding data were obtained from Bruker Ascend^{TM} 400 NMR spectrometer. The

structure and purity of the materials were identified by performing powder X-ray diffraction. The radiation source of Cu-Kα was used with a wavelength of 1.541 78 Å and the spectrum is recorded by using Rigaku Miniflex 600 diffractometer, between 5–40° (scan rate 1° min^{-1}). In addition, single-crystal X-ray diffraction study was performed by Bruker D8 with PHOTON 100 detector, with Cu-K$_\alpha$ ($\lambda = 1.541\,78$ Å) X-rays and data were collected between $6.21° \leqslant \theta \leqslant 59.06°$ at 296 K. The linear optical properties were performed between the wavelength 280 nm to 1100 nm using UV/VIS/NIR spectrometer and data/spectrum were collected from SHIMADZU UV1600 PC spectrometer. The defect states in the material were identified by using photoluminescence spectrometer and corresponding intensities were collected (FluoroMax-4CP spectrometer) between 410 nm and 600 nm. TGA/DTA analysis of 4M1PMS and 4BPMS crystals were performed by using SDT Q600 V20.9 build 20 instruments under nitrogen atmosphere between 25 °C and 600 °C, at a rate of 10° min^{-1}. The refractive index (n) of the single crystals were determined using Brewster's angle method, He-Ne laser (wavelength 632.8 nm). The grown single crystals were cut along different crystallographic directions and the surfaces are polished. These polished surfaces were used to reflect the laser beam for Brewster's angle measurement. The reflected beam was scanned by means of a photodetector. The observations were repeated with different angles of incidence. At the Brewster's angle (θ_p), the difference in intensity of the two polarized lights reflected from the surface, is maximum.

Laser damage threshold studies were performed (at 532 nm) by using frequency doubler with a source of Q-switched Nd-YAG laser (pulse width 6 ns). For powder SHG measurement, the capillary tube filled with powder crystals of uniform size, Q-switched Nd:YAG laser with a fundamental wavelength of 1064 nm and repetition rate of 10 Hz have been used. The energy 1.2 mJ/pulse and pulse width 10 ns was considered. Similarly, the nonlinear absorption/nonlinear refraction data were obtained from an open/closed aperure Z-scan technique. The experiment was carried out at 532 nm using Q-switched Nd-YAG laser source. The laser pulse width is about 7 ns and pulse repetition rate is 10 Hz. The beam focused using a lens of focal length of 25 cm and waist at the focus was about 21.8 μm. The thickness of the sample (1 mm) was smaller than Rayleigh length (2.8 mm).

3. Computational methods

The computations on 4M1PMS and 4BPMS have been performed using quantum chemistry program Gaussian09 package [23] using M06-2X functional [24] with 6-311++G (d.p) set basis [25, 26]. The first order hyperpolarizability (β), second-order hyperpolarizabilities (γ) and corresponding properties (α and $\Delta\alpha$) were calculated from finite field (FF) approach. This FF technique is used for the investigation of NLO co-efficient at molecular level and built a relationship on structure-property based on NLO parameters. When molecule is subjected to static electric field and considered as a weak system, the energy (E) is assumed and expressed to be in Taylor expansion series

$$E = E^0 - \sum_i \mu_i F^i - \frac{1}{2}\sum_{ij} \alpha_{ij} F^i F^j - \frac{1}{6}\sum_{ijk} \beta_{ijk} F^i F^j F^k - \frac{1}{24}\sum_{ijkl} \gamma_{ijkl} F^i F^j F^k F^l + \ldots$$

Where, E^0 is unperturbed energy of the molecule, μ_i is the dipole moment, F^i is field at the origin, α_{ij} is polarizability, β_{ijk} and γ_{ijkl} are the first order and second-order hyperpolarizability tensors respectively. The scalar factors: total dipole moment ($\mu_{tot} = \sqrt{\mu_x^2 + \mu_y^2 + \mu_z^2}$), mean polarizability ($\langle\alpha\rangle$) $\left(\text{where } \alpha = \frac{1}{3}(\alpha_{xx} + \alpha_{yy} + \alpha_{zz})\right)$ and anisotropy of polarizability $\left(\Delta\alpha = \frac{1}{\sqrt{2}}\sqrt{(\alpha_{xx} - \alpha_{yy})^2 + (\alpha_{yy} - \alpha_{zz})^2 + (\alpha_{zz} - \alpha_{xx})^2 + 6\alpha_{xy}^2 + 6\alpha_{yz}^2 + 6\alpha_{zx}^2}\right)$ can be calculated by considering either vector or tensor components. The electronic contribution of first order hyperpolarizability (β) and second order hyperpolarizability (γ) are given as follows,

$$\beta_{ele} = \sqrt{(\beta_{xxx} + \beta_{xyy} + \beta_{xzz})^2 + (\beta_{yyy} + \beta_{yzz} + \beta_{yxx})^2 + (\beta_{zzz} + \beta_{zxx} + \beta_{zyy})^2}$$

$$\gamma_{ele} = \frac{1}{5}[\gamma_{xxxx} + \gamma_{yyyy} + \gamma_{zzzz} + 2(\gamma_{xxyy} + \gamma_{xxzz} + \gamma_{yyzz})]$$

The detailed study of NLO parameters based on theoretical approach are discussed in the result section.

4. Results and discussion

4.1. Vibrational spectroscopy and ^{1}H-NMR studies

The presence of functional groups were identified and assigned to corresponding vibrational frequencies by using FT-IR and FT-Raman spectroscopic techniques. In both FT-IR and FT-Raman spectra the peaks above and close to 3000 cm^{-1} corresponding to C–H stretching vibrations, exhibit multiplicity band (moderate and

weak) as compared with aliphatic C-H stretching vibrations. This is due to reduction of negative charge on the carbon atom and reduction of dipole moments. The carbonyl group is most sensitive because the charge transfer takes place between the electron donors, electron acceptors to the carbonyl group.

In 4M1PMS, the high intense peak at 1662.0 cm^{-1} in infrared and less intense peak at 1661.64 cm^{-1} in the Raman spectra are assigned to C=O stretching vibrations. Similarly, the behavior and position of C=O stretching vibrations for 4BPMS are 1656.5 (IR) and 1656.91 (Raman). However, the strong intense peak in IR is due to dipole moment corresponding to C=O group, which is highly polar due to presence of multiply bonded groups and π-π stacking between the carbon and oxygen [27]. The predicted range for C=C is expected between 1620 to 1580 cm^{-1} in both FT-IR and FT-Raman. However, obtained intense vibrational modes for 4M1PMS and 4BPMS are 1601.2 cm^{-1}, 1595.8 cm^{-1} (IR) and 1600.02 cm^{-1} 1595.29 cm^{-1} (Raman). The given results match with theoretically predicted range and confirm that C=C is conjugated with C=O group. The vibrational modes are at 1368.4, 1151.32 in IR (4M1PMS) and 1368.27, 1150.70 in Raman (4M1PMS). Similarly, for 4BPMS, vibration modes are at 1388.1, 1151.1 in IR and 1376.82, 1154.50 in Raman, which were assigned to asymmetric SO$_2$ stretching vibrations. In both compounds, the peaks between 1500 and 1000 cm^{-1} correspond to the in-plane bending vibration and these planes are most likely to overlap with aromatic C-C vibration mode. On other hand, peaks below 1000 cm^{-1} are assigned to out-plane bending vibrations (wagging vibrations).

The presence of hydrogen atoms and purity of the initial compound was confirmed through ^{1}H NMR spectroscopic technique. The doublet peak for 4M1PMS at 7.935, 7.700 (J = 15.6 Hz) and for 4BPMS at 7.757, 7.430 (J = 15.6 Hz, 16 Hz) assigned to –CH=CH– belongs to E-configurations in both the samples. The spectrum shows that the significant peaks correspond to hydrogen atoms. Assignment of peaks are depicted below.

For 4M1PMS: Yield: 83% ; ^{1}H-NMR (400 Hz, δ, 3.357-DMSO): δ, 2.407 (s, 3 H of CH$_3$), δ, 2.43 (s, 3 H of CH$_3$), 7.935–7.896 (d, 1 H of –CH = CH–, J = 15.6 Hz), 7.700–7.661 (d, 1 H of –CH = CH–, J = 15.6 Hz). The other peaks assigned to aromatic rings.

For 4BPMS: Yield: 67%; ^{1}H-NMR (400 Hz, DMSO): δ, 2.461 (s, 3 H of CH$_3$), 7.757–7.717 (d, 1 H of –CH=CH–, J = 16 Hz), 7.430–7.391 (d, 1 H of –CH=CH–, J = 15.6 Hz). The other peaks are assigned to the aromatic rings.

Associated information corresponding to FT-IR and FT-Raman spectra for 4M1PMS and 4BPMS had been reported in supporting files (figures S1–S4 is available online at stacks.iop.org/MRX/7/055101/mmedia). In addition, corresponding 1H-NMR spectroscopy supporting files for 4M1PMS and 4BPMS are reported in figures S5 and S6.

4.2. Powder XRD

Powder XRD data was obtained to confirm the single-phase formation of the materials in bulk form for 4M1PMS and 4BPMS. The sharpness in peaks, which is obtained from the powder XRD pattern, provides an information about good crystallinity and phase formation of 4M1PMS and 4BPMS crystals. Figures 3(a) and 4(a) shows experimentally obtained powder XRD pattern and figures 3(b) and 4(b) shows simulated powder pattern obtained from single-crystal XRD (using Mercury software) in both 4M1PMS and 4BPMS. From the results, it is observed that experimental data is in good agreement with the simulated single crystal diffraction pattern, which confirms the formation of single-crystalline phase in the powder crystal samples.

In addition, the peaks were assigned from the h, k, l values in both 4M1PMS and 4BPMS. Furthermore, the crystal structure was determined by using EXPO2014 software [28] and inbuilt Program N-TREOR09 and DICVOL06 have been used for indexing and calculation of reflection-integrated intensities. Space group was identified by refinement-technique. All lattice parameters for 4M1PMS (unit cell and cell angle) were determined as follows, a = 6.26 Å, b = 7.30 Å and c = 43.58 Å; α = 90°, β = 90°, γ = 90° and cell volume (V) = 1993.4 Å^3. Similarly, for 4BPMS, lattice parameters are; a = 9.599 Å, b = 8.583 Å and c = 26.80 Å; α = 90°, β = 96.355°, γ = 90° and V = 2195.1 Å^3. All the refined parameters were in good agreement with single-crystal XRD data. From lattice parameters, it is noted that crystallographic system for 4M1PMS belongs to orthorhombic with $P2_12_12_1$ space group and 4BPMS belongs to monoclinic crystal system with $P2_1/n$ space group.

4.3. Single crystal XRD

The single crystal X-Ray diffraction study was performed and data were collected between 6.21° ⩽ θ ⩽ 59.06° using Bruker D8 with PHOTON 100 detector with a source Cu-K$_\alpha$ (λ = 1.541 78 Å). The reduction in data and processed by SAINT plus [29]; solving crystal structure: SHELXTL [30, 31] software; as it used for molecular graphics. The effect in absorption correction was performed through multi-scan technique, the direct method (SHELXTL) was performed to solve the crystal structure and refinement was performed by full-matrix least
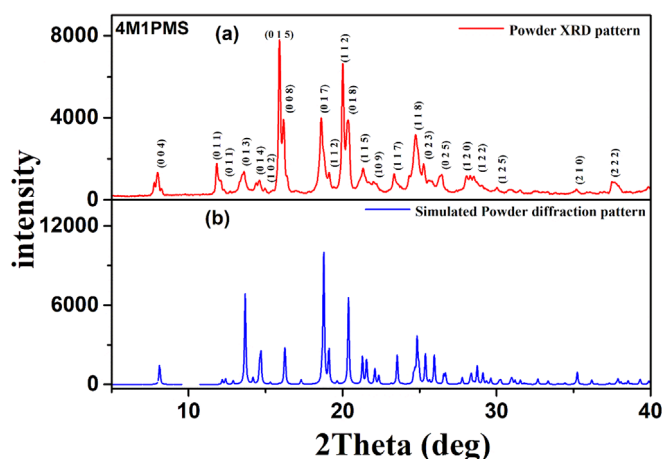
Figure 3. (a) bulk powder XRD pattern and (b) simulated powder diffraction pattern obtained from single-crystal XRD of 4M1PMS.
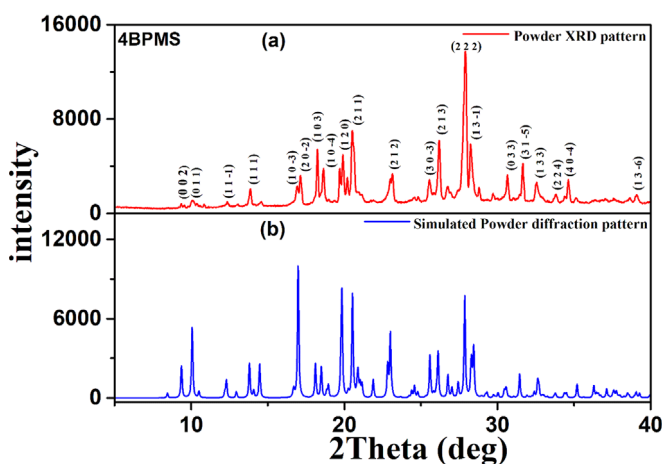

Figure 4. (a) bulk powder XRD pattern and (b) simulated powder diffraction pattern obtained from single-crystal XRD of 4BPMS.

square on F^2. All anisotropic thermal factors assign to refine the non-hydrogen atoms. Similarly, all hydrogen atoms positioned geometrically and refined by using riding model ($U_{iso}(H) = 1.2\ U_{equ}(C)$ or $1.5\ U_{equ}(C)$).

In 4M1PMS, Crystal symmetry belongs to $P2_12_12_1$ space group with orthorhombic class, which was identified from the calculated parameters; a $= 6.30(9)$ Å, b $= 7.22(11)$ Å and c $= 43.54(6)$ Å; $\alpha = 90°$, $\beta = 90°$, $\gamma = 90°$ and cell volume is 1984.1 (5) Å^3. In 4BPMS, the molecule belong to centrosymmetric class with a space group of $P2_1/n$ and its corresponding to monoclinic crystal system. The calculated lattice parameters are; a $= 10.9421(10)$, b $= 9.8831(9)$ and c $= 19.4000(18)$; $\alpha = 90°$, $\beta = 104.438(3)°$, $\gamma = 90°$ and cell volume is 2031.3 (3) Å^3. In general, material with non-centrosymmetry has both second-order and third order nonlinearity. In present study, the material 4M1PMS belongs to non-centrosymmetric class and is suitable for second harmonic generation (frequency doubling) applications. The centrosymmetric material 4BPMS is suitable for third-harmonic generation. In order to select the materials, it should have better response in chemical stability. Here, the chalcone derivative materials have trans-isomerism mechanism. However, both 4M1PMS and 4BPMS belong to trans-isomerism, which is confirmed by the coupling factor in NMR results (–CH = CH–). Generally, cis-isomers are less stable than trans-isomers. The packing diagram of 4M1PMS and 4BPMS molecules were generated by using MERCURY software [32] and ORTEP diagram of atomic labelled molecules (4M1PMS and 4BPMS) with 50% probability were shown in figures 5(a) and (b). The bond length between C14=C15 is 1.312 (5) Å (4M1PMS) and C14=C15 (–CH=CH–) is 1.326(4) Å (4BPMS) [figure 5] have good agreement with reported chalcone derivative materials [18–22, 33].

The structure related factors, which affect the nonlinear optical properties are given as conjugation length, presence of strong donor/acceptor electrons, charge transfer effect, intermolecular hydrogen bonds (C–H...O interactions) in the crystal packing with supramolecular layer, and so on. The charge transfer process is originated from the interactions of donor-acceptor group and the hydrogen bond interactions. The charge
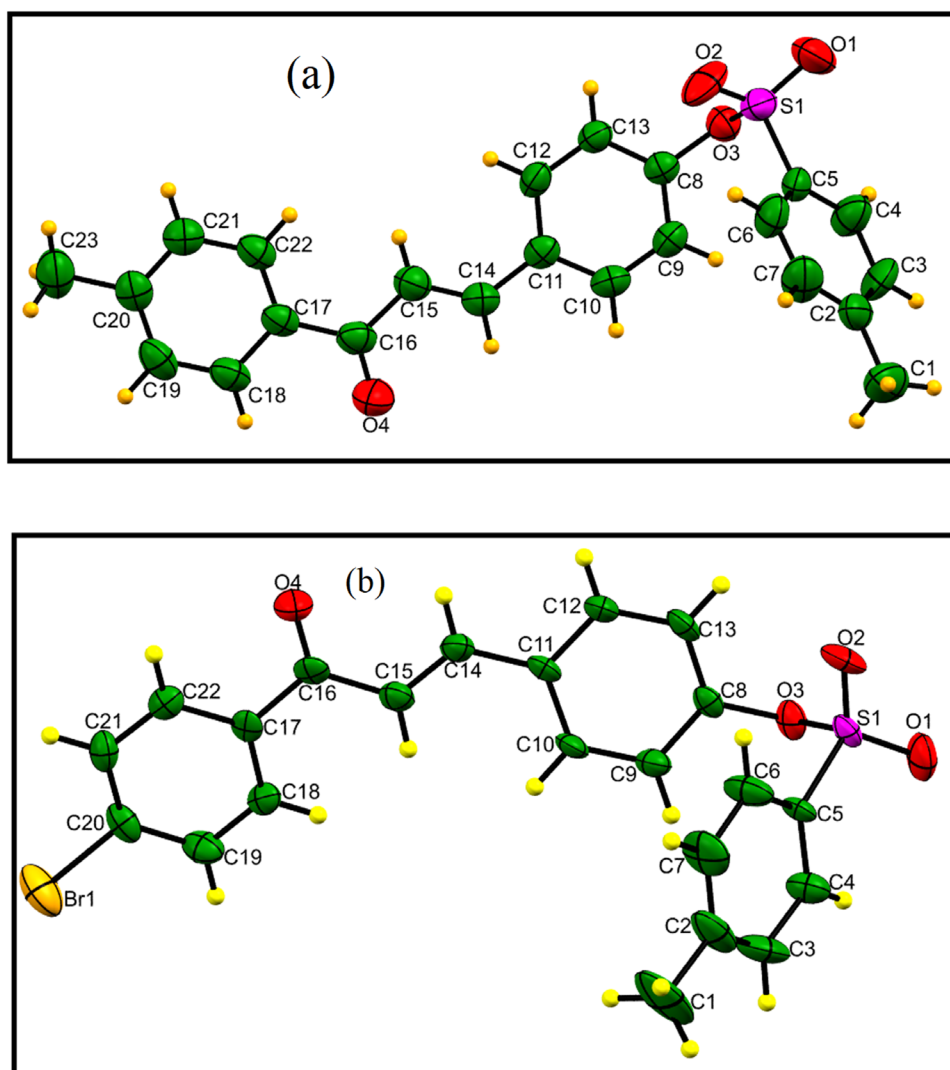
Figure 5. ORTEP diagram with thermal ellipsoid display (50% probability) of molecule (a) 4M1PMS (b) 4BPMS.

transfer between molecules through hydrogen bonding will generally favour a noncentrosymmetric packing (head-tail fashion). Moreover, extensive charge transfer within the molecule favours the inversion center packing, which induces large dipole moment [34].

The molecular planarity of 4M1PMS and 4BPMS have been measured from the dihedral angle between the aromatic rings. The dihedral angle between tosyloxy group and 4-methylphenyl ring is 32.81° (4M1PMS). Similarly, 4BPMS shows a dihedral angle of 62.82° between the tosyloxy group and 4-bromophenyl ring. From the results, it is observed that both molecules (4M1PMS and 4BPMS) have twisted structure and became nonplanar conformation in that, 4BPMS has more twisting behavior as compared to 4M1PMS and exhibit a distorted conformation. Moreover, the non-planar conformation with twisting molecular structures are due to different steric hindrance caused by donor electrons [35, 36]. Moreover, the sulfonyl group has tetrahedral geometry and is a stronger electron-withdrawing group than the carbonyl group [37]. Angles of the sulfonyl group O2–S1–O1 = 120.4 (2)° for 4M1PMS and O2–S1–O1 = 120.5 (2)° for 4BPMS. While the other angles are: S1-O3-C8 = 118.1(2)° for 4M1PMS and S1-O3-C8 = 119.7(2)° for 4BPMS. This indicated that S atoms in 4M1PMS and 4BPMS show distorted tetrahedral geometry and angle close to 120° [38]. Furthermore, the tosyloxy group in 4BPMS is twisted more from the enone group than that in 4M1PMS, which is confirmed by measuring mean plane angle between tosyloxy and enone group, which is 56.62°. On the other hand, 4M1PMS shows mean plane angle between tosyloxy and enone group as 38.02°. However, the mean plane angle between bromophenyl to carbonyl group is 4.30°. The mean plane angle (4.30°) in 4BPMS is smaller as compared to methyl phenyl - carbonyl group (10.45°). In general, the presence of sulfonyl group in the molecule limits the conjugation and the planarity maintained in the enone group through π-conjugation bridge [39, 40]. If the

molecules have elongated π-conjugation then the maximum absorbance peak is shifted to shorter wavelength, which is reported by Xiu Liu *et al* [41]. Both the 4M1PMS and 4BPMS have maximum absorbance peak shifted towards shorter wavelength (figure 8) as compared to 1-(4-methylphenyl)-3-(4-methoxyphenyl)-2-propen-1-one[42] and 3-(4-ethoxyphenyl)-1-(4-bromophenyl)prop-2-en-1-one [43]. The elongation of conjugation length is due to the presence of tosyloxy group in both 4M1PMS and 4BPMS. The deviation angle measured from the atom C8 in benzene ring attached to tosyloxy group is 85.95° for 4M1PMS molecule and 87.28° for 4BPMS molecule.

The selection of functional group in the molecules at a particular position influences the molecular stability. The intermolecular interaction between the molecules attributes to reasonably large complementarity of moderate-high molecular density in crystal packing for 4M1PMS and 4BPMS. It is noteworthy that, although weak C–H...O interactions contribute to the aggregation of molecules within the crystal, these interactions are responsible for the density of the molecule (1.314 g cm^{-3} for 4M1PMS and 1.495 g cm^{-3} for 4BPMS). The crystal-packing diagram of 4M1PMS and 4BPMS are shown in figures 6(a) and (b). The crystal packing is stabilized by various interactions of weak C–H...O, C–H...π and π...π stacking contacts, which represented as hydrophobic interactions or edge-face or T interactions reported by Almeida *et al* [44].

Here, the molecules 4M1PMS and 4BPMS have C–H...O interactions, which explain the process of obtaining the single crystals. The weak C–H...O or C–H...π interactions are ancillary interactions and optimization will determine the alignment of the crystal packing that helps in forming a stable dimolecular aggregate, which is the first stage of crystallization process reported by Dario Braga *et al* [45]. The crystal packing of 4M1PMS is stabilized by weak C9–H9...O2 interactions and aligned parallel with head-tail fashion arrangement, which is suitable for SHG applications. The intermolecular hydrogen bonding controls the molecular orientation and stability of the crystal packing. In 4M1PMS, tosyloxy group and methylphenyl group moieties engaged with the contribution of C1–H1C...O1 and C23–H23...O2 hydrogen bonding interactions lead to formation of infinite linear ribbons viewed along b-axis (figure 7(a)). Similarly, the molecule 4BPMS is stabilized by C–H...O and C–H...Br interactions. The supramolecular arrangements with weak C4–H4...O4 (C–H...O) interactions involved by tosyloxy group stabilize the crystal packing in 4BPMS. The interactions C22–H22...Br1, C18–H18...O1, and C19–H19...O2 are responsible for the unidimensional arrangement along a-axis (figure 7(b)). The charge transferred from the donor elements to supramolecular domain leads to delocalization in the upper energy levels and at the same time, intermolecular hydrogen bond interactions may help in extending charge transfer process to supramolecular domain in the excited state [34, 46]. Table 1 shows all crystallographic experimental data of 4M1PMS and 4BPMS. In addition, table 2 shows intermolecular interactions of the molecule 4M1PMS and 4BPMS. The crystal structure of these two molecules are deposited in CCDC (Cambridge crystallographic data center) which is available from the CCDC number 1900018 (4M1PMS) and 1900019 (4BPMS).

4.4. Linear optical properties

The linear optical properties provide an information about the types of electronic transition, localized states and electronic band structures. Figures 8(a) and (b) (inset graph), show prominent absorption characteristic behaviors of the materials. The sample taken in a 1 cm thick cuvette and measured by using methanol and DMF as internal standard solvents. The maximum absorption peak in UV region, found to be 308 nm (methanol) and 314 nm (DMF) for 4M1PMS and for 4BPMS maximum absorption characteristics peak at 310 nm (methanol) and 315 nm (DMF). The large absorption behavior in ultraviolet region, attributes to an unsaturated α, β-carbonyl group which may involve in n-π^*, π-π^* transitions. There are bathochromic shifts in both compounds as increase in solvent polarity (methanol > DMF). Polarity of methanol solvent is more when compared to DMF solvent. As a result, a small shift in methanol was observed and there is no significant absorption peak in the visible wavelength extended to near IR region (1100 nm) in both the samples. The entire transparency behavior in the visible and near IR shows that materials are efficient for NLO device applications. From transmittance, the relation was used to calculate absorption coefficient, $\alpha = 2.303\left[\log\left(\frac{1}{T}\right)\right]/d$ where, d is the thickness. Using the value of α the energy bandgap were extracted in both samples.

Tauc's plot [47], gives a relation between the energy band gap and absorption coefficient; $(\alpha h\nu) = A(h\nu - E_g)^n$ where, E_g is the energy bandgap of the material and n indicates transition type ($n = \frac{1}{2}$ for direct and $n = 2$ for indirect transitions) in the electronic band structure. The direct band gap is obtained by plotting the graph between $(h\nu)$ v/s $(\alpha h\nu)^2$. Calculated value of E_g found to be 3.7 eV (methanol) and 3.68 eV (DMF) for 4M1PMS and 3.65 eV (methanol) and 3.62 eV (DMF) for 4BPMS. The energy bandgap of the material decreases by increase in solvent polarity. The contribution of charge transfer absorbance and solvent polarity is the reason for energy band-gap variation. Due to charge transfer absorbance, the delocalization order is more in excited state than in ground state.
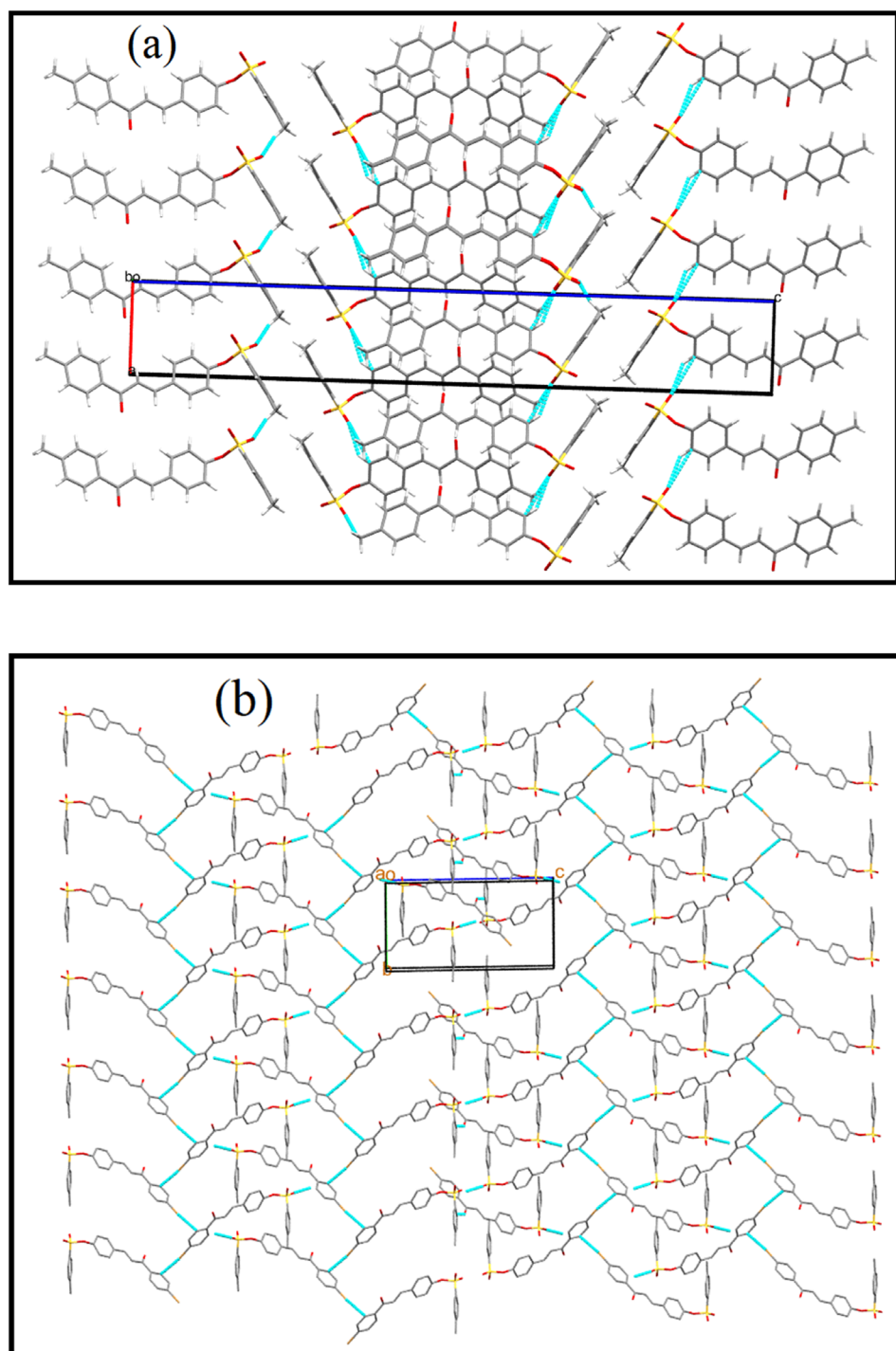
Figure 6. Partial packing diagram of the molecule (a) 4M1PMS viewed along b-axis (b) 4BPMS viewed along a-axis.

The presence of defect states were identified in the material by using photoluminescence (PL) spectroscopy (nondestructive technique). The room temperature PL with an excitation wavelength of 360 nm was used in both samples and observe the emission region between 410 and 600 nm. The PL signals shown in the visible region mainly involve by NBE (near band edge) and DLE (deep level emission). Figure 9 shows a broad emission spectrum for the sample 4M1PMS and 4BPMS in the range of 410 nm to 500 nm, which attributed to the presence of several transitions. The defect states corresponding to 4M1PMS are: (a) 449 nm in violet region (b) 456 nm, 461 nm, 466 nm, 480 nm and 490 nm in blue region (c) 568 nm in green region (d) 590 nm yellow region respectively. Similarly for 4BPMS, defects states are; (a) 449 nm in violet region (b) 456 nm, 461 nm, 466 nm, 471 nm, 480 nm and 490 nm in blue region (c) 568 nm in green region (d) 590 nm yellow region respectively. In both the samples, the defect states in violet and blue region are due to overlapping of the several emission peaks and broad region with defect states in blue region may be due to stacking faults [48, 49]. The
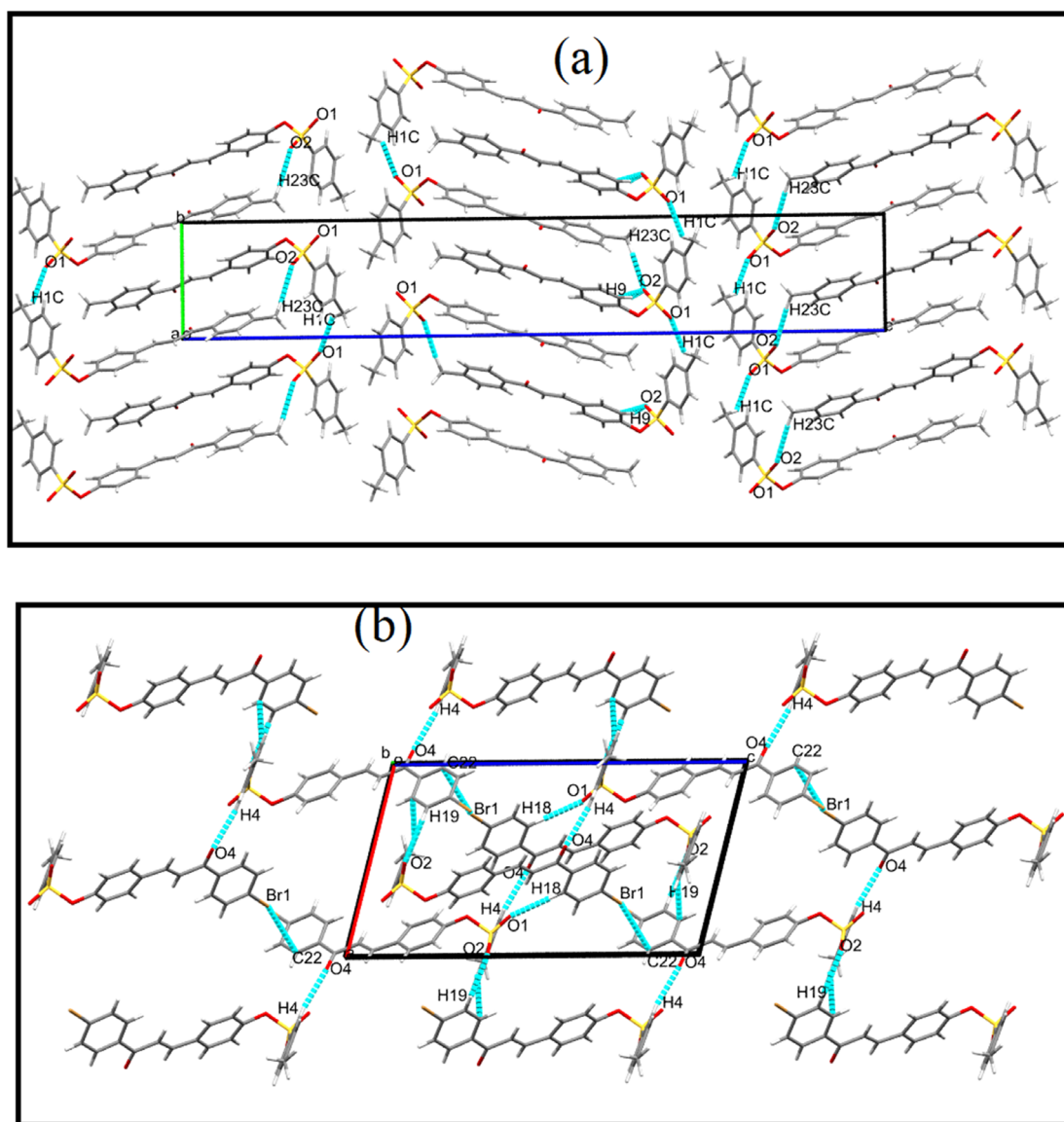
Figure 7. Hydrogen bond interaction involved by C–H…O (a) 4M1PMS viewed along a-axis (b) 4BPMS viewed along b-axis.

defects levels at green and yellow region have corresponding light emission property. Near band edge (437 nm [4M1PMS] 438 nm [4BPMS]) has shifted to longer wavelength due to presence of strong donor electrons in methyl and bromo groups attached to aromatic rings. Region of emission greater than energy bandgap shows that materials belong to the direct allowed transitions.

4.5. Thermal studies

The thermal stability and decomposition of the material have been identified using thermogravimetric (TG) and differential thermal (DT) analysis techniques. Significant endothermic peak at 138 °C and 143 °C correspond to melting point (MP) of the materials 4M1PMS and 4BPMS, respectively. There is no peak/transition until MP, which indicates that the materials can be used for device fabrication below the MP. Figures 10(a) and (b) represents the TGA/DTA spectrum of 4M1PMS and 4BPMS materials. In TG curve, 4M1PMS material is thermally stable up to 281 °C, 4BPMS is stable up to 285 °C, and there can be two-step weight changes in the materials. The first weight loss is 42.34 % (4M1PMS) and 28% (4BPMS) which were observed between the temperature range 290 °C–362 °C and 294 °C–357 °C, respectively. This attributes to the decomposition of the materials. The second weight loss were observed above 474 °C for 4M1PMS and above 483 °C for 4BPMS. The results of DTA in both the samples of 4M1PMS and 4BPMS shows a trace curve and peak 357 °C and 343 °C which correspond to decomposition of the initial compounds. Similarly, formation of gaseous phase were observed at 510 °C (4M1PMS) and 521 °C (4BPMS).
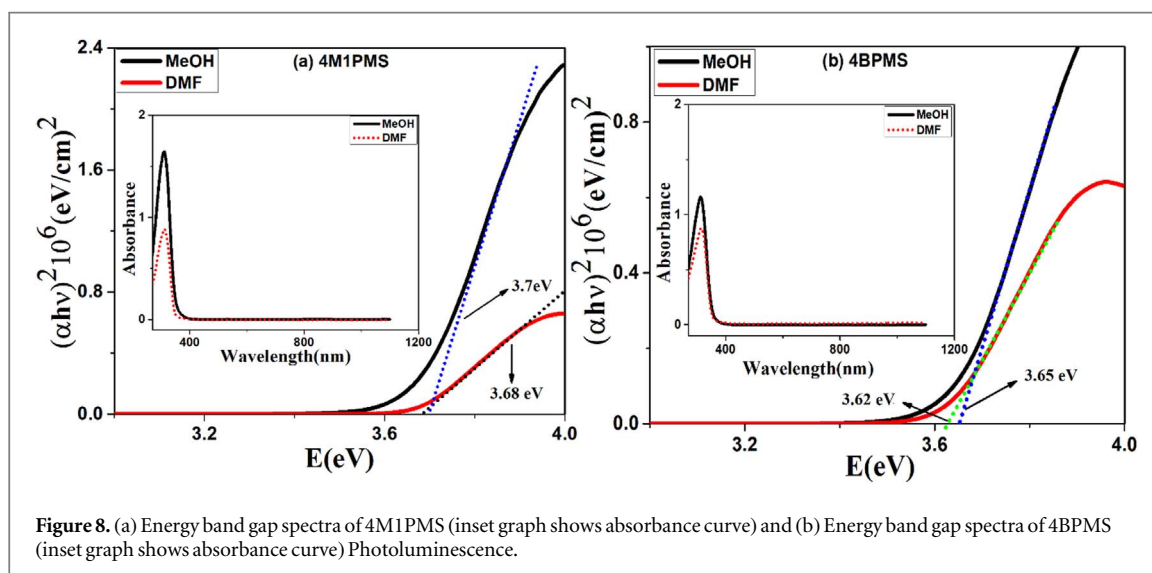
Figure 8. (a) Energy band gap spectra of 4M1PMS (inset graph shows absorbance curve) and (b) Energy band gap spectra of 4BPMS (inset graph shows absorbance curve) Photoluminescence.

Table 1. Crystallographic data and experimental details of chalcone derivatives.

CCDC number	1900018 (4M1PMS)	1900019 (4BPMS)
Molecular Formula	$C_{23}H_{20}O_4S$	$C_{22}H_{17}O_4BrS$
Formula Weight	392.45	457.33
Temperature (K)	296(2)	296(2)
Crystal size (mm^3)	0.23 × 0.24 × 0.26	0.22 × 0.24 × 0.26
Radiation type	Cu-K$_\alpha$	Cu-K$_\alpha$
Radiation Wavelength	1.54 Å	1.54 Å
Radiation source	fine-focus sealed tube	fine-focus sealed tube
Unit cell dimensions (Å)	a = 6.3045(9), b = 7.2283(11) and c = 43.538(6)	a = 10.9421(10), b = 9.8831(9) and c = 19.4000(18)
Cell angles (°)	$\alpha = 90, \beta = 90, \gamma = 90$	$\alpha = 90, \beta = 104.438(3), \gamma = 90$
Volume (Å^3)	1984.1 (5)	2031.7 (3)
Reflections measured	2641	2700
Observed reflections (I > 2σ(I))	2629	2616
Extinction coefficient	0.037(3)	0.025(2)
Absorption co-efficient (μ) in (mm^{-1})	1.667	3.933
Density (g cm^{-3})	1.314	1.495
h, k, l values	6, − 6; 8, − 7; 48, −47	12, − 12; 10, − 10; 21, −21
Parameters	256	255
Goodness of fit on F^2	1.135	1.055
R_all, R_obs	0.0478, 0.0477	0.0775, 0.0768
wR$_2$_all, wR$_2$_obs	0.1185, 0.1184	0.1889, 0.1866
$\nabla\rho$ (min, max)/e Å^{-3}	− 0.228, 0.178	−1.751, 0.982

Table 2. Intermolecular interaction of 4M1PMS and 4BPMS.

Molecules	D-H...A	D-H (Å)	H...A (Å)	D...A (Å)	D-H...A (°)
4M1PMS	C9-H9...O2	0.93	2.380	3.157	140.98
	C1-H1C...O1	0.96	2.674	3.440	137.10
	C23-H23C...O2	0.96	2.719	3.661	167.25
4BPMS	C18-H18...O1	0.931	2.430	3.313	158.50
	C4-H4...O4	0.93	2.489	3.385	161.72
	C19-H19...O2	0.93	2.666	3.333	129.19
	C22-H22...Br1	0.93	3.768	3.525	97.97

Symmetry code: 1/2−x, −y, 1/2+z, 1/2+x,1/2−y, −z and −x,1/2+y,1/2−z (**4M1PMS**); 1/2−x,1/2+y,1/2−z, −x, −y, −z and 1/2+x,1/2−y,1/2+z (**4BPMS**).
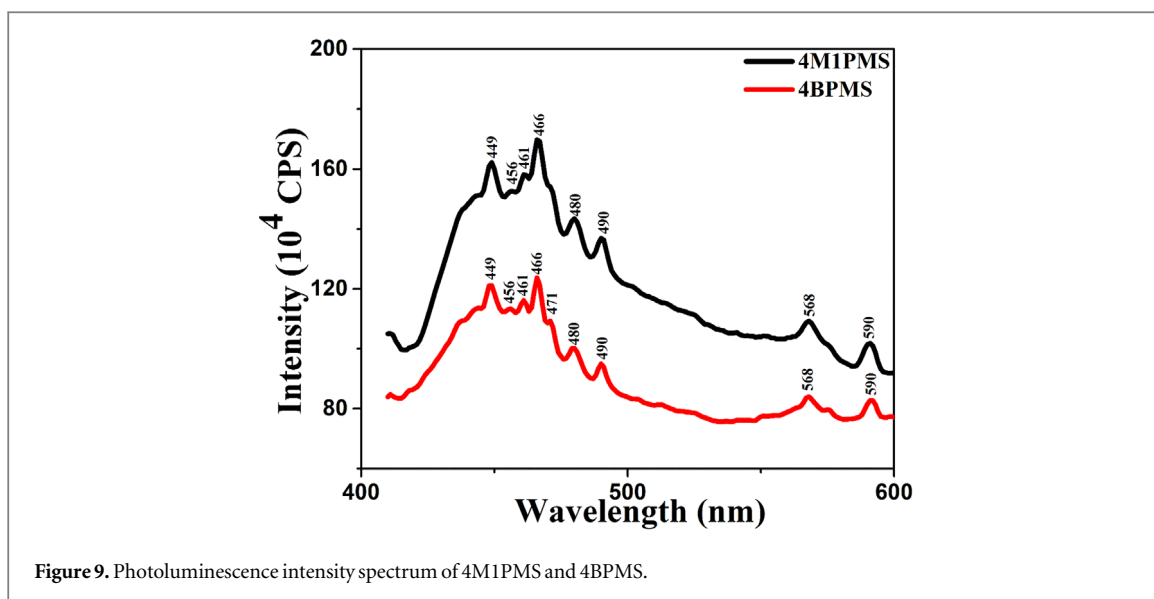
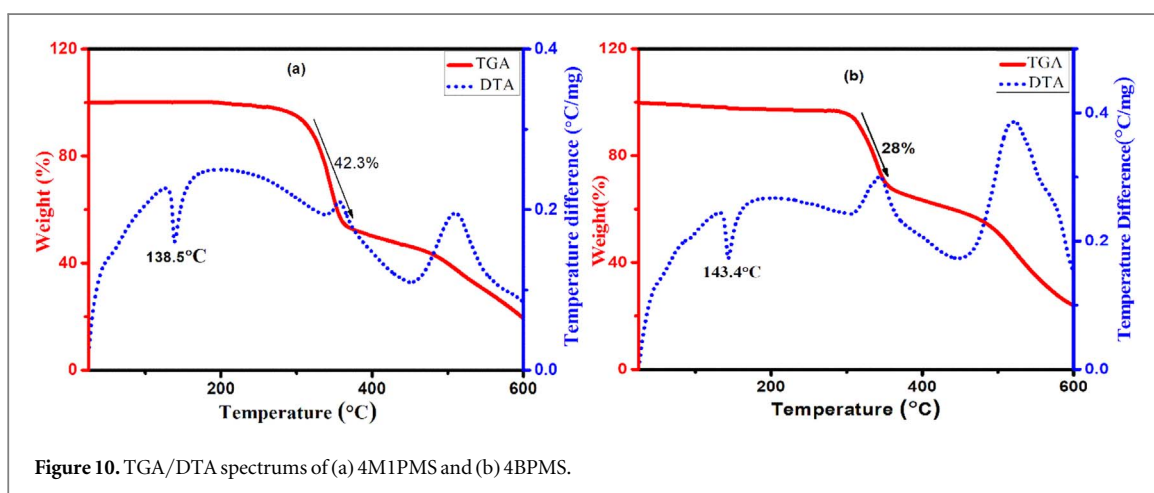**Figure 9.** Photoluminescence intensity spectrum of 4M1PMS and 4BPMS.

Figure 10. TGA/DTA spectrums of (a) 4M1PMS and (b) 4BPMS.

4.6. Refractive index of 4M1PMS and 4BPMS

The refractive index of the materials 4M1PMS and 4BPMS were determined by Brewster's angle method and is given by $n = \tan \theta_p$; where, θ_p is the polarizing angle. The refractive index of 4M1PMS and 4BPMS crystals are 1.60 and 1.59, which are comparable with other organic materials [20, 50]. The precise measurement of refractive index is required for nonlinear optical and optoelectronic applications [51, 52]. Refractive index is the strong tool for determining many figure of merit of optical component such as filters, reflectors, and resonators [52, 53].

4.7. Laser damage threshold study

For the selection of efficient material for device applications, crystal should not have damaged surfaces with high power laser. In order to select the material for laser applications, laser damage threshold (LDT) studies have been performed.

The well-polished crystal with flat face (thickness 2.1 mm - 4M1PMS and 1.4 mm - 4BPMS) were used for LDT measurement. Here, the output intensity controlled over by filters, which delivers intense light to the material. The sample position is fixed near the converging lens with a focal length of 4 cm. Following relation is used to calculate surface damage threshold value i.e.,

$$\text{Power density} \ (P_d) = \frac{E}{\tau \pi r^2} \text{GW cm}^{-2} \tag{1}$$

Where, E (energy) is in mJ, τ (pulse width) is in ns and r (beam spot size) is in mm.

LDT value of 4M1PMS and 4BPMS are found to be 9.64 GW cm^{-2} and 8.72 GW cm^{-2}, respectively. 4M1PMS and 4BPMS have better radiation tolerance as compared with other chalcone derivative material BMP [54] ($\lambda = 1064$ nm, 4.16 GW cm^{-2}), methoxy-ANC ($\lambda = 532$ nm, 3.98 GW cm^{-2}) and ethoxy-ANC [55]

Table 3. Electronic contribution parameters of dipole moment (μ_{tot} in Debye) and anisotropy of polarizability (α and $\Delta\alpha$ in $10^{-24}e$ su) first order hyperpolarizability (β_{tot} in 10^{-30} esu) and second order hyperpolarizability (γ in 10^{-40} esu).

Electronic contribution parameters		4M1PMS		4BPMS	
μ	β_{yyy}	3.607	−0.993	5.593	−0.563
μ_x	β_{xxz}	1.603	−1.893	1.512	7.105
μ_y	β_{xyz}	3.164	0.937	5.383	0.614
μ_z	β_{yyz}	0.655	0.036	−0.149	−0.226
α_{xx}	β_{xzz}	67.62	−0.661	67.07	0.791
α_{yy}	β_{yzz}	44.31	0.465	43.03	0.331
α_{zz}	β_{zzz}	29.03	−0.042	35.09	−0.099
α_{xy}	β_{tot}	−0.319	12.74	5.254	14.96
α_{xz}	γ_{xxxx}	6.085	61.76	4.238	−119.5
α_{yz}	γ_{yyyy}	−2.252	−22.25	−3.781	79.30
$\langle\alpha\rangle$	γ_{zzzz}	46.99	−39.52	48.40	40.23
$\Delta\alpha$	γ_{xxyy}	122.05	−156.4	119.8	−75.42
β_{xxx}	γ_{xxzz}	9.574	53.52	13.41	−25.45
β_{xxy}	γ_{yyzz}	7.912	11.28	−4.72	2.803
β_{xyy}	γ_{tot}	1.295	−36.65	−1.820	−39.23

($\lambda = 532$ nm, 5.28 GW cm^{-2}), 4MPNP [56] ($\lambda = 532$ nm, 1.2 GW cm^{-2}) and PDBA [46] ($\lambda = 532$ nm, 4 GW cm^{-2} and $\lambda = 1064$ nm, 8 GW cm^{-2}). This study reveals that the crystals in the present report have better optical damage resistance; hence, the crystals can be promoted for laser applications.

4.8. Electronic contributions: NLO activity

For the selection of efficient materials for device applications, multidisciplinary effort and knowledge of both experimental and theoretical NLO studies is very much essential. Therefore, quick and inexpensive way (theoretical) have been applied to predict NLO parameters. In order to understand, electronic polarization and underlying structure property relationship, it is necessary to establish the theoretical aspects. All the parameters corresponding to electronic polarization, dipole moment, hyperpolarizability tensors obtained from the frequency in Gaussian output file are reported in table 3. It is noticed that value of dipole moment (μ) for both 4M1PMS and 4BPMS were 3.607 Debye and 5.593 Debye, respectively. The charge transfer which takes place in bromo-substituted derivative (4BPMS), is more as compared to methyl-substituted derivative (4M1PMS). The y-component has maximum dipole moment compared with other two phases [$\mu_y = 3.164$ Debye (4M1PMS) and 5.383 Debye (4BPMS)]. The average polarizability values (α) were found to be 46.99×10^{-24} esu (4M1PMS) and 48.40×10^{-24} esu (4BPMS). Among all polarization directions, the component α_{xx} is more than the other two polarizability component in both the molecules. The values of α_{xx} is found to be 67.62×10^{-24} esu (4M1PMS) and 67.07×10^{-24} esu (4BPMS). This exhibits maximum polarization along x-direction in both the molecules. The first order hyperpolarizability (β) values for 4M1PMS and 4BPMS were found to be 12.74×10^{-30} esu and 14.96×10^{-30} esu. The order of magnitude β were comparable with those of other chalcone derivatives [27, 57, 58] and found 36.5 times (4M1PMS) and 43 times (4BPMS) that of urea [59] (3.48×10^{-31} esu). All the electronic contribution NLO parameters were compared and depicted in table 4. The component β_{xxx} (9.574×10^{-30} esu) in 4M1PMS is reasonably larger than any other hyperpolarizability components in terms of β. The smaller value of β, mainly from the molecular packing, takes place along x–axis which affects the nonlinear susceptibility [3, 60]. Moreover, the delocalization of electron from donor to acceptor makes a molecule highly polarizable and those delocalized electron clouds are perpendicular to the bond axis. Similarly, in 4BPMS, β_{xxx} (13.41×10^{-30} esu) component is high; this exhibits charge transfer which takes place along the x-direction as a result, π-orbitals were involved in the ICT (inter-molecular charge transfer) process. The second-order hyperpolarizability exhibits third-order nonlinear process (γ). If optical frequency is dominated by few more order, then two-photon resonance can occur, contributing to second-order hyperpolarizability. The calculated values of γ for 4M1PMS and 4BPMS were found to be -36.65×10^{-40}esu and -39.23×10^{-40}esu. According to quantum optics, the positive sign of γ is due to self-focusing effect and negative sign corresponds to self–defocusing effect. As compared with 4M1PMS, 4BPMS is more interesting due to large negative $\gamma -$ value. Those γ negative materials are extensively studied,

Table 4. Comparison of electronic contribution parameters of μ, α, $\Delta\alpha$, β and γ with some NLO molecules.

Molecular parameter	μ (debye)	α (10^{-24}esu)	$\Delta\alpha$ (10^{-24}esu)	β (10^{-30}esu)	γ (10^{-40}esu)
4M1PMS	3.607	46.99	122.05	12.74	−36.65
4BPMS	5.593	48.40	119.8	14.96	−39.23
3Br4MSP [27]	5.233	41.90	138.2	79.03	−26.01
2,4,5-TMBC [57]	5.955	46.69	39.53	21.13	—
4BPDPP [58]	3.130	9.622	—	8.319	—

due to larger sensitivity by small change in the structure. These type of molecules possess intense electron correlation, which results in better controllable system for nonlinear optical devices.

5. Nonlinear optcial properties

5.1. Second order and third order nonlinear optical properties

Kurtz and Perry technique [61], is a well-known method for powder SHG measurements. The powder sample was taken in a capillary tube and exposed to laser radiation (fundamental beam of Nd-YAG laser). The emission of green light obtained from the powder crystalline sample is focused through a lens, to photomultiplier tube detector (Hamamatsu-R 2059), which collects the second harmonic wave signal from the material after being filtered out the fundamental signals by using IR filters. Further, generated signal was converted into electric signals which can be observed in oscilloscope (Tektronix-TDS 3052B). The amplitude of the signal is compared with those for standard materials like urea and KDP crystals. The material 4M1PMS has good second-order nonlinearity due to its non-inversion symmetry matrix behaviour. Second-harmonic generation efficiency of 4M1PMS (48 mV) is 0.76 times that of urea (63 mV) and 2.2 times that of KDP (22 mV) crystals. The crystal shows less efficiency as compared to urea due to large band dispersion, which affects NLO response according to Dadsetani *et al* [3]. Similarly, 4BPMS (SHG = 0) does not have SHG factor due to its centrosymmetric nature.

For the characterization of third-order nonlinear optical properties, The solution of the material (in DMF) was taken in 1 mm thick cuvette and was studied by means of the single beam Z-scan technique. This technique was developed by Sheik-Bahae [62, 63]. The study of nonlinear optical properties such as, nonlinear absorption (NLA) and nonlinear refraction (NLR) uses open/closed aperture Z-scan technique. For nonlinear optical absorption/refraction, the contribution of solvent has been separately investigated, because, rotational contribution in solvent affects the nonlinear optical parameters, which is negligible in the present investigation [64].

In open aperture condition, a cuvette-containing solution was placed in front of the detector without placing aperture. The normalized transmittance for open aperture $\left(T(z) = 1 - \frac{1}{2\sqrt{2}}\beta_{eff} I_o L_{eff} \frac{1}{1 + \frac{Z^2}{Z_0^2}}\right)$ is obtained by fitting with two-photon absorption model. Figures 11(a) and (b) shows the open aperture Z-scan data with theoretical fit of two-photon model for the sample of 4M1PMS and 4BPMS, respectively. The nonlinear absorption coefficient (β) values were obtained from the point where intensity peak is maximum. From experimental data, the value of β for 4M1PMS and 4BPMS were found to be 5.73 cm GW^{-1} and 5.6 cm GW^{-1} at 1.81 GW cm^{-2} respectively. The contribution of nonlinear absorption attributed from the two-photon absorption (TPA) is confirmed from theoretical fit to the experimental data. The behavior of NLA curve represents RSA (reverse saturable absorption). The RSA material has ultra-fast response time behavior. TPA leads optical nonlinearity in the materials. As a result, the nonlinear optical absorptive centre in the unit volume (N_0) is assumed to find two-photon absorption coefficient (σ_2), which is co-relative factor of NLA co-efficient ($\beta = \sigma_2 N_0$) [10, 65]. The molecular TPA cross-section (σ_2') is given by, $\sigma_2' = \sigma_2 h\nu$ where, σ_2' is in cm^4.s/photon and $h\nu$ is in joule. The values of σ_2 and σ_2' for 4M1PMS is found to be 9.52 $\times$ 10^{-19} cm^4 GW^{-1} and 3.55 $\times$ 10^{-46} cm^4.s/photon, respectively. Similarly, for 4BPMS, the values are 9.29 $\times$ 10^{-19} cm^4 GW^{-1} and 3.47 $\times$ 10^{-46} cm^4.s/photon, respectively. Figures 12(a) and (b) show optical limiting behaviour curve for 4M1PMS and 4BPMS where the data are extracted from open aperture Z-scan results. Inter band electron transition and reverse saturable absorptions are responsible for optical limiting behaviour. Optical limiters are high transmitter for low fluence and opaque at high fluence laser beam. The nonlinear optical mechanism causes optical limiting behavior from the effect of RSA, TPA, free carrier absorption and nonlinear scattering. Optical limiting behavior caused from RSA has fast response time as compared with other mechanisms because it involves electronic transitions. In order to select best optical limiter, material should have low limiting threshold value. The optical limiting threshold value are found to be 0.572 GW cm^{-2} and 0.587 GW cm^{-2} for 4M1PMS and 4BPMS, respectively.
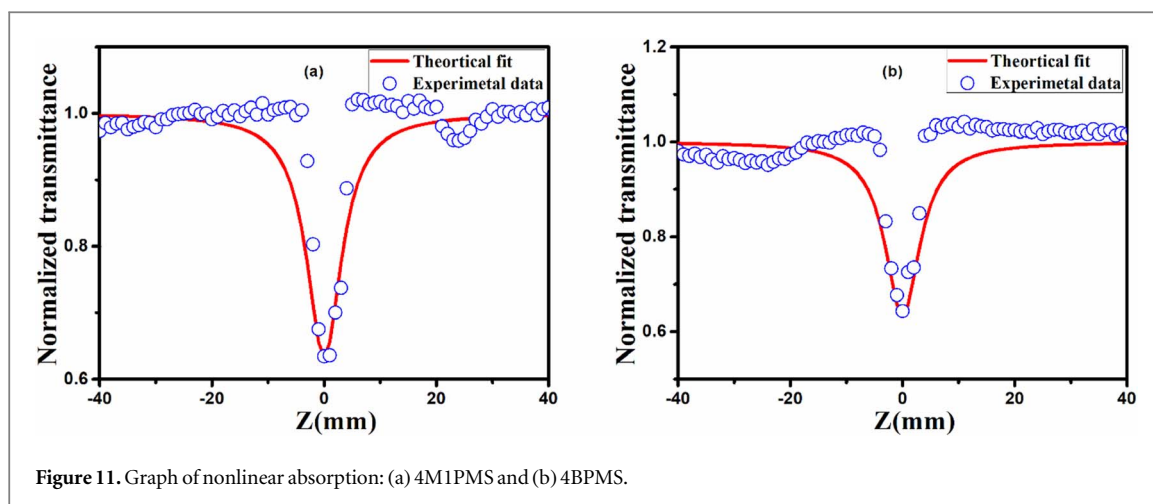
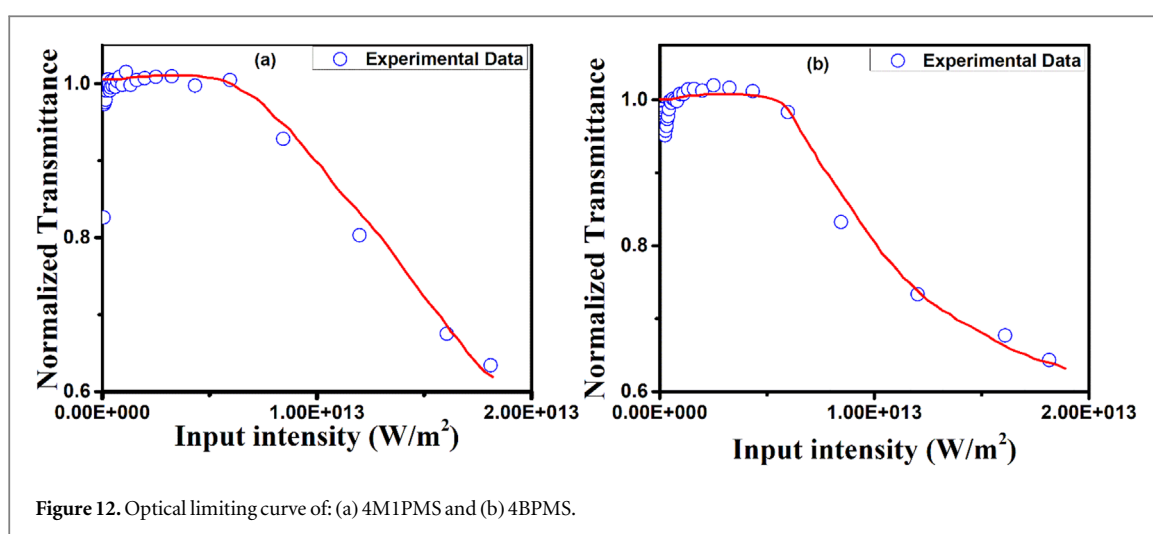**Figure 11.** Graph of nonlinear absorption: (a) 4M1PMS and (b) 4BPMS.

Figure 12. Optical limiting curve of: (a) 4M1PMS and (b) 4BPMS.

For measuring of nonlinear refraction using closed aperture, the sample is placed near to the detector and moved across the region +Z to −Z positions. Pyroelectric detector is used to collect transmitted intensity. Nonlinear refraction is collected in closed aperture, whereas pure nonlinear refraction is obtained by dividing this by nonlinear absorption data (open aperture Z - scan data). The behavior of the curve moved from peak to valley has evidence for self-defocusing and negative nonlinear refraction. Figures 13(a) and (b) represents the nonlinear refraction curve for 4M1PMS and 4BPMS. The nonlinear refractive index is represented in terms of NLR coefficient and is given by,

$$n_2(esu) = (cn_0/40\pi)\gamma \, (\text{m}^2/\text{W}) \tag{2}$$

$$\gamma = \frac{\Delta\varphi_0 \lambda}{2\pi L_{eff} I_0} \tag{3}$$

Where n_0 and $\Delta\varphi_0$ represents linear refractive index ($n_0 = 1.6 \, and \, 1.59$) and nonlinear phase shift. The value of γ is found to be $1.413 \times 10^{-17} \text{m}^2/\text{W}$ for 4M1PMS and $1.07 \times 10^{-17} \text{m}^2/\text{W}$ for *4BPMS*. The delocalization of electron in the molecule enhances the second-order hyperpolarizability ($\gamma_h = \frac{\chi^{(3)}}{N_c L^4}$) and γ_h is dependent factor for third-order nonlinear optical susceptibility. In the above equation, L is the local field factor ($L = \frac{n_0^2 + 2}{3}$) and N_c is density of molecule. All the calculated parameters corresponding to nonlinear absorption and nonlinear refraction of 4M1PMS and 4BPMS are enumerated in table 5. In table 6, the results of 4M1PMS and 4BPMS were compared with organic/inorganic/thin films based materials. It is noted that the value of $\chi^{(3)}$ is reasonably larger than that for small conjugation based organic molecular system [50, 66, 67] but two-fold magnitude order greater than those for inorganic materials [68, 69]. Furthermore, results are comparable with organic/organometallic based thin films and dyes materials [70–73].
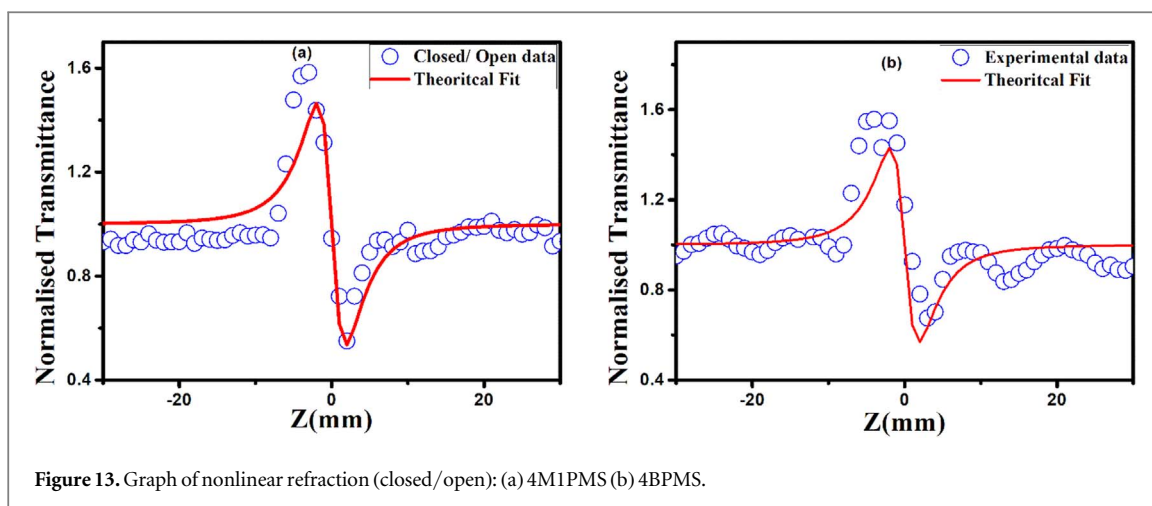
Figure 13. Graph of nonlinear refraction (closed/open): (a) 4M1PMS (b) 4BPMS.

Table 5. Nonlinear optical parameters of 4M1PMS and 4BPMS crystals at 532 nm.

Sample	n_2 (esu) $\times 10^{-11}$	β (m/W) $\times 10^{-11}$	Re $(\chi^{(3)})$(esu) $\times 10^{-11}$	Im $(\chi^{(3)})$(esu) $\times 10^{-11}$	$\chi^{(3)}$ (esu) $\times 10^{-11}$	γ_h (esu) $\times 10^{-31}$
4M1PMS	−5.40	5.73	−0.918	0.157	0.931	6.69
4BPMS	−4.06	5.6	−0.686	0.152	0.726	2.25

Table 6. Comparison $\chi^{(3)}$ values of few organic/inorganic/thin films based material.

Materials	(λ) (nm)	$\chi^{(3)}$ (esu) $\times 10^{-14}$	Reference
Organic crystal (Z-scan-solution)			
4M1PMS work		931	Present
4BPMS work		726	Present
1-(5-chlorothiophen-2-yl)-3-(2,3- dimethoxyphenyl)prop-2-en-1-one		17.04	[49]
(2E)-1-(3-fluoro-4-methoxyphenyl)-3-(4-methoxyphenyl) prop-2-en-1-one	532 nm	204.8	[66]
(2E)-3-(4-chlorophenyl)-1-(3-fluoro-4-methoxyphenyl)prop-2-en-1-one		759.0	[66]
(2E)-3-(5-bromo-2-thienyl)-1-(4-nitrophenyl)prop-2-en-1-one		352.0	[67]
Inorganic crystals (Z-scan-crystal)			
potassium dihydrogen phosphate (KDP)	532 nm	8.34	[68]
deuterated potassium dihydrogen phosphate (DKDP)		6.51	[68]
KBe$_2$BO$_3$F$_2$	355 nm	9.4	[69]
Organic/organometallic (THG-thin film)			
Naphtho[2,1-d:6,5-d′]bis([1–3]dithiazole		2100	[70]
Bis-(8-hydroxyquinolinato)zinc	355 nm	116	[71]
8-Hydroxyquinoline copper(II)		132	[71]
Tris-(8-hydroxyquinoline)aluminum		96	[71]
Dyes			
1,5-Diaminoanthraquinone	532 nm	726	[72]
Terphenyl derivatives			
S1		12.5	
S2	532 nm	31	[73]
S3		19.4	
S4		22.9	

6. Conclusions

Nonlinear optical materials (4M1PMS and 4BPMS) have been synthesized and their single crystals were grown by slow solvent evaporation technique. The number of hydrogen atoms and materials purity were confirmed through ^{1}H-NMR spectroscopy technique. The functional groups were identified from the vibrational

spectroscopic studies (FT-IR and FT-Raman). The crystal structure, the molecular structure and its parameters for 4M1PMS and 4BPMS were obtained from single-crystal X-ray diffraction studies. The crystal structures are stabilized by C–H...O and π...π intermolecular interactions. The materials have small change in the energy band gap due to different solvent polarity. In PL-spectra, both the samples have sharp defect levels in broad emission region, which exhibits corresponding light emission property. In addition, the materials (4M1PMS and 4BPMS) are thermally stable up to 281 °C and 285 °C. The crystals have high resistance power and corresponding LDT values are found to be 9.64 GW cm^{-2} (4M1PMS) and 8.72 GW cm^{-2} (4BPMS), respectively. Theoretical simulations on NLO study at molecular level helps to predict NLO response at macroscopic level. The molecular hyperpolarizability is reliable which gives an intense attention to consider nonlinear optical materials. The 4M1PMS material has noninversion symmetry matrix, due to which it has SHG efficiency 2.2 times that of KDP. The results of nonlinear absorption in the materials were due to TPA mechanism. The values of β were 5.73 cm GW^{-1} and 5.6 cm GW^{-1} which correspond to 4M1PMS and 4BPMS, respectively, at 1.81 GW cm^{-2}. Materials have better optical limiting response and values were found to be 0.572 GW cm^{-2} (4M1PMS) and 0.587 GW cm^{-2} (4BPMS). The values of nonlinear optical susceptibility for 4M1PMS and 4BPMS were found to be in the order of 10^{-11} esu, which makes the crystals potential candidates for NLO applications.

Acknowledgments

Conflicts of interest

Authors declares that there is no conflict of interest in the present article.

ORCID iDs

Vinay Parol ⓘ https://orcid.org/0000-0002-1493-5232
A N Prabhu ⓘ https://orcid.org/0000-0002-1005-0461
N K Lokanath ⓘ https://orcid.org/0000-0003-2773-2247
Md Abu Taher ⓘ https://orcid.org/0000-0002-0652-3318
Sri Ram G Naraharisetty ⓘ https://orcid.org/0000-0002-6407-2017

References

[1] Bosshard C H, Bosch M, Liakatas I, Ja¨ger M and Gunter P 2000 *In Nonlinear Optical Effects and Materials* ed P Gunter (Heidelberg, Germany: Springer- Verlag)

[2] Bosshard C H, Sutter K, Pretre P H, Hulliger J, Florsheimer M, Kaatz P and Gunter P 1995 *Organic Nonlinear Optical Materials* (Newark, NJ: Gordon and Breach Publishers)

[3] Dadsetani M and Omidi A R 2015 A DFT study of linear and nonlinear optical properties of 2-Methyl-4-nitroaniline and 2-amino-4-nitroaniline crystals *J. Phys. Chem. C* **119** 16263–75

[4] Saripalli R K, Katturi N K, Soma V R, Bhat H L and Elizabeth S 2017 Non-critically phase-matched second harmonic generation and third order nonlinearity in organic crystal glucuronic acid γ-lactone *J. Appl. Phys.* **122** 223110

[5] Whitten A E, Jayatilaka D and Spackman M A 2006 Effective molecular polarizabilities and crystal refractive indices estimated from x-ray diffraction data *J. Chem. Phys.* **125** 174505

[6] de laTorre G, Vazquez P, Agullo-Lopez F and Torres T 2004 Role of structural factors in the nonlinear optical properties of phthalocyanines and related compounds *Chem. Rev.* **104** 3723–50

[7] Mutter L, Brunner F D, Yang Z, Jazbinšek M and Günter P 2007 Linear and nonlinear optical properties of the organic crystal DSTMS *J. Opt. Soc. Am. B* **24** 2556

[8] Yang Z, Mutter L, Stillhart M, Ruiz B, Aravazhi S, Jazbinsek M, Schneider A, Gramlich V and Günter P 2007 Large-size bulk and thin-film stilbazolium-salt single crystals for nonlinear optics and THz generation *Adv. Funct. Mater.* **17** 2018–23

[9] Bailey R T, Bourhill G, Cruickshank F R, Pugh D, Sherwood J N and Simpson G S 1993 The linear and nonlinear optical properties of the organic nonlinear material 4-nitro-4′-methylbenzylidene aniline *J. Appl. Phys.* **73** 1591–7

[10] He G S, Weder C, Smith P and Prasad P N 1998 Optical power limiting and stabilization based on a novel polymer compound *IEEE J. Quantum Electron.* **34** 2279–85

[11] He G S, Tan L S, Zheng Q and Prasad P N 2008 Multiphoton absorbing materials: molecular designs, characterizations, and applications *Chem. Rev.* **108** 1245–330

[12] Bouit P A, Wetzel G, Berginc G, Loiseaux B, Toupet L, Feneyrou P, Bretonnière Y, Kamada K, Maury O and Andraud C 2007 Near IR nonlinear absorbing chromophores with optical limiting properties at telecommunication wavelengths *Chem. Mater.* **19** 5325–35

[13] Pramodini S, Sudhakar Y N, Selvakumar M and Poornesh P 2014 Studies on third-order optical nonlinearity and power limiting of conducting polymers using the z-scan technique for nonlinear optical applications *Laser Phys.* **24** 045408

[14] Anto R J, Sukumaran K, Kuttan G, Rao M N A, Subbaraju V and Kuttan R 1995 Anticancer and antioxidant activity of synthetic chalcones and related compounds *Cancer Letters* **97** 33–7

[15] Lahtchev K L, Batovska D I, Parushev S P, Ubiyvovk V M and Sibirny A A 2008 Antifungal activity of chalcones: a mechanistic study using various yeast strains *Eur. J. Med. Chem.* **43** 2220–8

[16] Choi D, Park J C, Lee H N, Moon J H, Ahn H W, Park K and Hong J 2018 *In vitro* osteogenic differentiation and antibacterial potentials of chalcone derivatives *Mol. Pharmaceutics* **15** 3197–204

[17] Shubhalaxmi, Pathak L, Ananda K and Bhat K S 2016 Synthesis of focused library of novel aryloxyacids and pyrazoline derivatives: molecular docking studies and antimicrobial investigation *Cogent Chemistry* **2** 1141388

[18] Tejkiran P J, Teja M S B, Siva P S, Sankar P, Philip R, Naveen S, Lokanath N K and Rao G N 2016 D-A- p -D synthetic approach for thienyl chalcones – NLO – a structure activity study *Journal of Photochemistry & Photobiology, A: Chemistry* **324** 33–9

[19] Fichou D, Watanabe T, Takeda T, Miyata S, Goto Y and Nakayama M 1988 Influence of the ring-substitution on the second harmonic generation of chalcone derivatives *Japan. J. Appl. Phys.* **27** L429–30

[20] Prabhu S R, Jayarama A, Chandrasekharan K, Upadhyaya V and Ng S W 2017 Synthesis, growth, structural characterization, Hirshfeld analysis and nonlinear optical studies of a methyl substituted chalcone *J. Mol. Struct.* **1136** 244–52

[21] Vinaya P P, Prabhu A N, Subrahmanya Bhat K and Upadhyaya V 2019 Synthesis, growth and characterization of a long-chain π-conjugation based methoxy chalcone derivative single crystal; a third order nonlinear optical material for optical limiting applications *Opt. Mater.* **89** 419–29

[22] Vinaya P P, Prabhu A N, Subrahmanya Bhat K and Upadhyaya V 2018 Design, growth and characterization of D-π-A-π-D based efficient nonlinear optical single crystal for optical device applications *J. Phys. Chem. Solids* **123** 300–10

[23] Frisch M J *et al* 2010 *Gaussian 09, Revision A. 02* (Wallingford CT: Gaussian, Inc.)

[24] Becke A D 1993 Density-functional thermochemistry. III. The role of exact exchange *J. Chem. Phys.* **98** 5648–52

[25] Petersson G A, Bennett A, Tensfeldt T G, Al-Laham M A, Shirley W A and Mantzaris J 1988 A complete basis set model chemistry. I. The total energies of closed-shell atoms and hydrides of the first-row elements *J. Chem. Phys.* **89** 2193–218

[26] Stephens P J, Devlin F J, Chabalowski C F and Frisch M J 1994 *Ab initio* calculation of vibrational absorption and circular dichroism spectra using density functional force fields *J. Phys. Chem.* **98** 11623–7

[27] Kumar A, Kumar R, Gupta A, Tandon P and D'silva E D 2017 Molecular structure, nonlinear optical studies and spectroscopic analysis of chalcone derivative (2E)-3-[4-(methylsulfanyl) phenyl]-1-(3-bromophenyl) prop-2-en-1-one by DFT calculations *J. Mol. Struct.* **1150** 166–78

[28] Altomare A, Rizzi R, Corriero N and Falcicchio A 2013 EXPO2013 : a kit of tools for phasing crystal structures from powder data *J. Appl. Crystallogr.* **46** 1231–5

[29] APEX, APEX2, SMART, SAINT, SAINT-Plus: Bruker 2012 *Program Name(s)* (Madison, Wisconsin, USA: Bruker AXS Inc.)

[30] Sheldrick G M 2015 SHELXT - integrated space-group and crystal-structure determination *Acta Cryst* **71** 3–8

[31] Sheldrick G M 1997 *SHELXL-97 Program Automatic Solution of Crystal Structures* (Göttingen, Germany: University of Göttingen)

[32] Macrae C F *et al* 2008 Mercury CSD 2.0 - new features for the visualization and investigation of crystal structures *J. Appl. Crystallogr.* **41** 466–70

[33] Prabhu A N, Jayarama A, Sankolli R, Guru Row T N and Upadhyaya V 2011 2E)-1-(5-Chloro-thio-phen-2-yl)-3-(2,3-dimethoxyphen-yl)prop-2-en-1-one *Acta Crystallogr. Sect. E Struct. Reports Online* **67** o2665

[34] Cole J M, Howard J A K and McIntyre G J 2001 Influence of hydrogen bonding on the second harmonic generation effect: neutron diffraction study of 4-nitro-4′-methylbenzylidene aniline *Acta Crystallogr., Sect. B: Struct. Sci* **57** 410–4

[35] Tao S S, Fang Y, Yi Y J, Bing H Y and Lin S Y 2018 The remarkable enhancement of two-photon absorption in pyrene based chalcone derivatives *Opt. Mater.* **86** 331–7

[36] Go M, Wu X and Liu X 2012 Chalcones: an update on cytotoxic and chemoprotective properties *Curr. Med. Chem.* **12** 483–99

[37] Chataigner I, Panel C, Gérard H and Piettre S R 2007 Sulfonyl vs. carbonyl group: which is the more electron-withdrawing? *Chem. Commun.* 3288–90

[38] Andleeb H, Khan I, Bauzá A, Tahir M N, Simpson J, Hameed S and Frontera A 2018 A comparative experimental and theoretical investigation of hydrogen-bond, halogen-bond and π-π interactions in the solid-state supramolecular assembly of 2- and 4-formylphenyl arylsulfonates *Acta Crystallographica Section C: Structural Chemistry* **74** 816–29

[39] Li Y, Tang M, Wang J, Su H, Liu R, Chen J and Zhu H 2018 Synthesis, crystal structure and luminescent properties of p-diphenylsulphone compounds with different substituents *Opt. Mater.* **86** 449–54

[40] De Castro M R C, Aragão Â Q, Da Silva C C, Perez C N, Queiroz D P K, Júnior L H K Q, Barreto S, De Moraes M O and Martins F T 2016 Conformational variability in sulfonamide chalcone hybrids: crystal structure and cytotoxicity *J. Braz. Chem. Soc.* **27** 884–98

[41] Liu X, Yang Z, Wang D and Cao H 2016 Molecular structures and second-order nonlinear optical properties of ionic organic crystal materials *Crystals* **6** 158

[42] Crasta V, Ravindrachary V, Bhajantri R F and Gonsalves R 2004 Growth and characterization of an organic NLO crystal: 1-(4-methylphenyl)-3-(4-methoxyphenyl)-2-propen-1-one *J. Cryst. Growth* **267** 129–33

[43] Patil P S, Bhumannavar V M, Bannur M S, Kulkarni H N and Bhagavannarayana G 2013 Second harmonic generation in some donor-acceptor substituted chalcone derivatives *J. Cryst. Process Technol.* **3** 108–17

[44] Almeida L R, Anjos M M, Ribeiro G C, Valverde C, Machado D F S, Oliveira G R, Napolitano H B and De Oliveira H C B 2017 Synthesis, structural characterization and computational study of a novel amino chalcone: a potential nonlinear optical material *New J. Chem.* **41** 1744–54

[45] Braga D, Grepioni F, Maini L and D'Agostino S 2017 Making crystals with a purpose; a journey in crystal engineering at the University of Bologna *IUCrJ* **4** 369–79

[46] Ravindra H J, Kiran A J, Dharmaprakash S M, Satheesh Rai N, Chandrasekharan K, Kalluraya B and Rotermund F 2008 Growth and characterization of an efficient nonlinear optical D-π-A-π-D type chalcone single crystal *J. Cryst. Growth* **310** 4169–76

[47] Tauc J, Grigorovici R and Vance A 1996 Optical properties and electronic structure of amorphous germanium *Phys. Stat. Sol.* B **15** 627–37

[48] Gutiérrez-Argüelles D, Portillo M C, Portillo-Moreno O, Palomino-Merino R, Mora-Ramírez M A, Rubio-Rosas E, Hernández-Téllez G and Gutiérrez-Pérez R 2019 Maxwell-Boltzmann statistics applied in the study of photoluminescent emission bands in the (S)-(-)-1-(4-bromophenyl)-N-1,2,3,4-(tetrahydro-1-naphthyl)methanimine organic crystals *Opt. Mater.* **96** 109307

[49] Ramírez-Márquez J, Portillo-Moreno O, Palomino-Merino R, Rubio-Rosas E, Mora-Ramírez M A, Hernández-Téllez G, Moreno-Morales G E and Gutiérrez-Pérez R 2019 Blue and green emission bands in the enantiopure (S)-(-)-1-[(1-phenyl)-N-(biphen-2-yl)methylidene]ethylamine: morphological, structural and optical properties *Optik* **185** 331–8

[50] Prabhu A N, Upadhyaya V, Jayarama A and Subrahmanya Bhat K 2013 Synthesis, growth and characterization of π-conjugated organic nonlinear optical chalcone derivative *Mater. Chem. Phys.* **138** 179–85

[51] Gieseking R L, Mukhopadhyay S, Risko C, Marder S R and Brédas J L 2014 25th anniversary article: design of polymethine dyes for all-optical switching applications: guidance from theoretical and computational studies *Adv. Mater.* **26** 68–84

[52] Schubert E F, Kim J K and Xi J Q 2007 Low-refractive-index materials: a new class of optical thin-film materials *Phys. Status Solidi Basic Res.* **244** 3002–8

[53] Anis M and Muley G G 2016 Single crystal growth and enhancing effect of glycine on characteristic properties of bis-thiourea zinc acetate crystal *Phys. Scr.* **91** 1–8

[54] Arunkumar K and Kalainathan S 2017 Synthesis, growth and characterization of organic nonlinear optical single crystal 1,3-bis(4-methoxyphenyl)prop-2-en-1-one (BMP) by vertical Bridgman technique *Opt. Laser Technol.* **89** 143–50

[55] Mathew E, Salian V V, Hubert Joe I and Narayana B 2019 Third-order nonlinear optical studies of two novel chalcone derivatives using Z-scan technique and DFT method *Opt. Laser Technol.* **120** 105697

[56] Raghavendra S, Chidankumar C S, Jayarama A and Dharmaprakash S M 2015 1-[4-(methylsulfanyl) phenyl]-3-(4-nitrophenyl) prop-2-en-1-one: a reverse saturable absorption based optical limiter *Mater. Chem. Phys.* **149** 487–94

[57] Shkir M, Muhammad S, AlFaify S, Irfan A, Patil P S, Arora M, Algarni H and Jingping Z 2015 An investigation on the key features of a D-π-A type novel chalcone derivative for opto-electronic applications *RSC Adv.* **5** 87320–32

[58] Asiri A M, Karabacak M, Sakthivel S, Al-Youbi A O, Muthu S, Hamed S A, Renuga S and Alagesan T 2016 Synthesis, molecular structure, spectral investigation on (E)-1-(4-bromophenyl)-3-(4-(dimethylamino)phenyl)prop-2-en-1-one *J. Mol. Struct.* **1103** 145–55

[59] Adant C, Dupuis M and Bredas J L 1995 *Ab initio* study of the nonlinear optical properties of urea: electron correlation and dispersion effects *Int. J. Quantum Chem.* **56** 497–507

[60] Castet F and Champagne B 2002 Simple scheme to evaluate crystal nonlinear susceptibilities: semiempirical AM1 model investigation of 3-Methyl-4-nitroaniline crystal *The Journal of Physical Chemistry A* **105** 1366–70

[61] Kurtz S K and Perry T T 1968 A powder technique for the evaluation of nonlinear optical materials a powder technique for the evaluation of nonlinear optical materials *J. Appl. Phys.* **39** 3798

[62] Sheik-Bahae M, Said A A, Wei T H, Hagan D J and Van Stryland E W 1990 Sensitive measurement of optical nonlinearities using a single beam *IEEE J. Quantum Electron.* **26** 760–9

[63] Sheik-Bahae M, Said A A and Van Stryland E W 1989 Stryland, high-sensitivity, single-beam n_2 measurements *Opt. Lett.* **14** 955–7

[64] Rau I, Kajzar F, Luc J, Sahraoui B and Boudebs G 2008 Comparison of Z-scan and THG derived nonlinear index of refraction in selected organic solvents *J. Opt. Soc. Am.* B **25** 1738

[65] Sutherland R L, Brant M C, Heinrichs J, Rogers J E, Slagle J E, McLean D G and Fleitz P A 2005 Excited-state characterization and effective three-photon absorption model of two-photon-induced excited-state absorption in organic push-pull charge-transfer chromophores *J. Opt. Soc. Am.* B **22** 1939

[66] Shekhara T C, Kumar C S C, Patel K N G, Shyang T, Dharmaprakash S M, Ramasami P, Umar Y, Chandraju S and Kheng C 2017 Optical nonlinearity of D-A- p -D and D-A- p -A type of new chalcones for potential applications in optical limiting and density functional theory studies *J. Mol. Struct.* **1143** 306–17

[67] Patil P S, Maidur S R, Shkir M, Alfaify S, Ganesh V, Krishnakanth K N and Rao S V 2018 Crystal growth and characterization of second- and third-order nonlinear optical Chalcone derivative: (2E)-3-(5-bromo-2-thienyl)-1-(4-nitrophenyl)prop-2-en-1-one *J. Appl. Crystallogr.* **51** 1035–42

[68] Wang D, Li T, Wang S, Wang J, Wang Z, Xu X and Zhang F 2016 Study on nonlinear refractive properties of KDP and DKDP crystals *RSC Adv.* **6** 14490–5

[69] Li F-Q *et al* 2012 Investigation of third-order optical nonlinearity in KBe$_2$BO$_3$F$_2$ crystal by Z-scan *Appl. Phys.* B **108** 301–5

[70] Takauji K, Suizu R, Awaga K, Kishida H and Nakamura A 2014 Third-order nonlinear optical properties and electroabsorption spectra of an organic biradical, [naphtho[2,1- d:6,5- d ′]bis([1,2,3]dithiazole)] *J. Phys. Chem.* C **118** 4303–8

[71] Popczyk A, Aamoum A, Migalska-Zalas A, Płóciennik P, Zawadzka A, Mysliwiec J and Sahraoui B 2019 Selected organometallic compounds for third order nonlinear optical application *Nanomaterials* **9** 254

[72] Sreenath M C, Hubert Joe I and Rastogi V K 2018 Third-order optical nonlinearities of 1,5-diaminoanthraquinone for optical limiting application *Opt. Laser Technol.* **108** 218–34

[73] Kamath L, Manjunatha K B, Shettigar S, Umesh G, Narayana B, Samshuddin S and Sarojini B K 2014 Investigation of third-order nonlinear and optical power limiting properties of terphenyl derivatives *Opt. Laser Technol.* **56** 425–9